6. Amelinckx, S., Zhang, X. B., Bernaerts, D., Zhang, X. F., Ivanov, V. and Nagy, J. B., A formation mechanism for catalytically grown helix-shaped graphite nanotubes. *Science*, 1994, **265**, 635–639.
7. Ajayan, P. M., Ravikumar, V. and Charlier, J. C., Surface reconstruction and dimensional changes in single-walled carbon nanotubes. *Phys. Rev. Lett.*, 1998, **81**, 1437–1440.
8. Charlier, J. C., Defects in carbon nanotubes. *Acc. Chem. Res.*, 2002, **35**, 1063–1069.
9. Terrones, M., Banhart, F., Grobert, N., Charlier, J. C., Terrones, H. and Ajayan, P. M., Molecular junctions by joining single-walled carbon nanotubes. *Phys. Rev. Lett.*, 2002, **89**, 075505 (1–4).
10. Deepak, F. L., Govindaraj, A. and Rao, C. N. R., Improved synthesis of carbon nanotubes with junctions and of single-walled carbon nanotubes. *J. Chem. Sci.*, 2006, **118**, 9–14.
11. Szabó, A., Fonseca, A., Nagy, J. B., Lambin, Ph. and Biro, L. P., Structural origin of coiling in coiled carbon nanotubes. *Carbon*, 2005, **43**, 1628–1633.
12. Frisch, M. J. *et al.*, Gaussian 03, Revision C-02, Gaussian Inc., Pittsburg, PA, 2003.

ACKNOWLEDGEMENTS. This study was supported in part by a grant from Defence Materials and Stores Research and Development Establishment (DMSRDE), Kanpur. We thank Drs D. Roy and K. Mukhopadhyay of DMSRDE Kanpur for valuable discussions. C.N.R. thanks the UGC, New Delhi for a senior research fellowship and N.S. thanks the DST, New Delhi for a J. C. Bose fellowship.

Received 28 July 2006; revised accepted 7 November 2006

Molecular tensegrity: predicting 1,3–*X*– – –*X* distance in gas-phase MX_n ($n \leq 4$) compounds from atomic sizes

Parthasarathy Ganguly

Physical Chemistry Division, National Chemical Laboratory, Homi Bhabha Road, Pune 411 008, India

This article extends an earlier definition[1] and use of molecular tensegrity for obtaining quantitatively the 1,3-non-bonded distances in gas-phase MX_2 compounds to nearly 160 gas-phase MX_n ($n \leq 4$) inorganic compounds (including those of transition metal elements), once a transferable 'core' atomic size is specified. The simple principles behind this methodology (involving only linear equations), its quantitative character, its transparency, its portability and its generality account very simply for molecular geometry in such compounds without requiring earlier theoretical methodologies. We also establish clear distinction in the prescription for obtaining the 1,3-distance when *M* is an atom of a metallic or insulating element.

Keywords: Atomic size, gas phase, molecular tensegrity, non-bonded distance.

THE Fuller notion[2] of tensegrity structures has structural elements that are held together by compressive and tensile elements that balance each other. Such a notion is expected to hold for all length scales, as a general principle. Fuller–Snelson tensegrity structures using (incompressible) struts and (tensile) cables describe well the qualitative features of the role of cell and tissue architecture in the dynamics of complex biological systems[3]. A 'molecular tensegrity'[4] that determines, say, the mechanical stability of the structure of isolated gas-phase MX_2 has recently been proposed, taking advantage of a free-atom-like $\mu = 0$ condition[5,6] in which atoms in molecules may be treated independent of each other. The molecular tensegrity structure is obtained from simple mechanical relationships between atomic sizes that contribute to interatomic distances 'without requiring to know the (quantum) mechanics of the way the $\mu = 0$ state is reached from a $\mu \neq 0$ state'.

For an isolated MX_n molecule, the mutual influences of 1,2-bonded (attractive) M–X distance, d_{M-X}, and 1,3-non-bonded (repulsive) X– – –X distances, d_{X-X}, is expressed (eq. (3)) as a tensegrity factor (similar to the tolerance factor in solids[7,8]) that forms the quantitative basis for molecular tensegrity. 1,2-Interatomic distance, d^{n0}_{MX}, has been expressed as[5,9] an universal function of 'core' (small compared to interatomic distances) empirical[9] atomic sizes, r_G as

$$d^{n0}_{MX} = CR^{+}_{0}(M)/F_S(M) + CR^{-}_{0}(X) = [C^{+}_{0} r_G(M) + D^{+}_{0}]/F_S(M) + C^{-}_{0} r_G(X) + D^{-}_{0}, \quad (1)$$

with $CR^{\pm}_0 = C^{\pm} r_G + D^{\pm}_0$, and $C^{+}_0 = 2.24$, $C^{-}_0 = 2.49$, $D^{-}_0 = 111$ pm and $D^{+}_0 = -37$ pm. The term[10] $F_S(M)$ is associated[10] with decrease in atomic sizes or bond lengths due to the presence of n_v 'unsaturated' valence electrons. We take[10] $F_S = 1$ ($n_v = 0$) for all M except for transition metal MX_3 ($n_v = 1$) and MX_4 compounds ($n_v = 2$). The superscript, $\pm$, refers to charge-transfer states CR^{+}_0 and CR^{-}_0 in (eq. 1). The size $CR^{-}_0(X)$ is close to the ionic radii in solids[9] and is different from the van der Waals' radius[11], $r_{VDW} \neq CR^{-}_0(X)$. The non-bonded distance, d^{00}_{XX} is expected to be

$$d^{00}_{XX} = 2KCR^{-}_0(X). \quad (2)$$

Unless otherwise mentioned, we take $K = 1$ hereafter. Equations (1) and (2) are required to define an ideal 'tensegrity' factor[4], $t^{\pm}_{n0}$, as

$$t^{\pm}_{n0} = d^{n0}_{MX}/d^{00}_{XX}. \quad (3)$$

We have expressed an experimental quantity[4] F_S (obs) as

$$F_S(\text{obs}) = d_{XX}(\text{obs})/d^{00}_{XX} \equiv d_{XX}(\text{obs})/2CR^{-}_0(X). \quad (4)$$

A plot of F_S (obs) vs $t^{\pm}_{n0}$ (Figure 1) for all gas-phase MX_2, MX_3 and MX_4 compounds[12,13] (X = atom of insulating element) two nearly linear relationships of the type

$$F_S(\text{obs}) = A - Bt^{\pm}_{n0} \quad (5)$$

are obtained (Figure 1) which we refer to as type I and type II. From the ratios of the two slopes in Figure 1 we

*For correspondence. (e-mail: patch_ganguly@rediffmail.com)

find F_S (obs)$^{(II)}/F_S$ (obs)$^{(I)}$ ~ 1.12 for the same $t^{\pm}_{n0}$. In general, type I MX_n compounds have M = atom of s-block metal, (met(s) in Figure 1), or transition metal dihalides (TM(n = 2)), while type II compounds have M as an atom of an insulating element (ins), p-block metal (met(p)) or transition metal MX_3 or MX_4 compounds (TM(n > 2)). The compounds AlH_2, MH_4 (M = Sn and Pb) are better described as type II compounds (see also Figure 3).

The relationships in Figure 1 may be understood from Fuller's original qualitative description[2] of tensegrity, which considers 'continuous, tensional behaviors' as in a stretched membrane of a filled balloon. The 'critical proximities that show up physically' are 'repellings' which keep the molecular network constituting the balloon membrane stretched outwardly in all directions. The vital aspect now is that the 'repellings' have to be balanced by attractive or tensile elements to obtain a tensegrity structure. Atoms of finite size in molecules may be treated as these 'balloons'. When the hurly burly of the balancing act (complex quantum chemical mathematics) between positive (repulsion, kinetic energy) and negative (attraction) multipart contributions to the energy from different charged particles in the molecule is done, the positions of atoms in a molecule become fixed relative to others for a given environment. A tensegrity model may then be applied to molecular structure. The geometrically simplifying Fuller feature of the balloon membrane model is the notion of 'paired oppositely accelerated' particles caroming around in 'most comfortable great circles', three of which intersect to give vertices of two spherical octahedra, one octahedron for each opposing direction. We simply accept the notion of 'octahedron' representing a 'standard' state. All molecules in their stable state are treated as tensegrity structure made up of struts and tensile elements. We examine these molecules in terms of an ideal octahedron irrespective of their actual topological features.

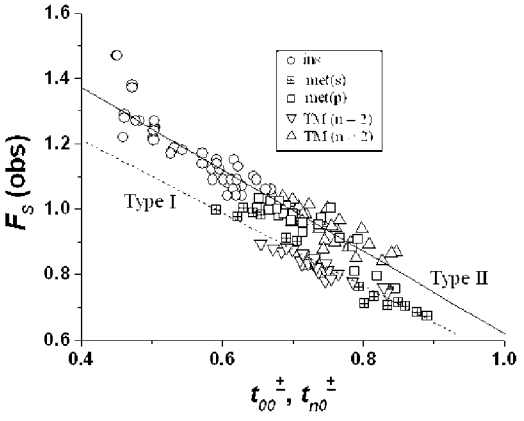

Figure 1. Plot of F_S (obs) (eq. (4)) vs the tolerance factor, $t^{\pm}_{n0}$ (eq. (3)) for gas-phase MX_2, MX_3 and MX_4 compounds. Dotted line: Type I compounds (M = metal); F_S (obs) = 1.66(0.04) – 1.12(0.5) $t^{\pm}_{00}$, R = –0.96, SD = 0.03. Full line: Type II compounds (M = insulator); F_S(obs) = 1.87(0.02) – 1.25(0.4) $t^{\pm}_{00}$; R = –0.96, SD = 0.04.

The seemingly linear relationships (eq. (5)) in Figure 1 may be understood from the simple geometrical limits of octahedral structures, which also helps to place on a quantifiable basis the notion of tensegrity in molecules. Thus, we examine eq. (4) in terms of the ratio of atomic sizes, $(CR_0^+(M)/CR_0^-(X)$. The ratio $CR_S^+(M)/CR_S^-(X) = 0.414$, geometrically represents the lower limit for stable octahedral coordination in ligand close-packed scenarios. This close-packing description is quite different from that envisaged by Gillespie *et al.*[13,14]. Writing eq. (3) as $t^{\pm}_{00} \equiv 0.5(CR_0^+(M)/CR_0^-(X) + 1)$ we require from eq. (5), F_S (obs) = 1 when $t^{\pm}_{00}$ = 1/1.414 = 0.707. From the best fit of F_S(obs) vs $t^{\pm}_{n0}$ for type II compounds (Figure 1) we find F_S(obs) ~ 1.01 when $t^{\pm}_{00}$ = 0.707. Ideally, we prefer F_S(obs) = (2 – 1.414$t^{\pm}_{00}$) and obtain from eqs (2), (3) and (5)

$$d_{XX}\,(\text{calcd}) = 2\kappa KCR_0^-(X)/(2 - 1.414t^{\pm}_{00}), \qquad (6)$$

κ (~ 1) may be treated as an effective dielectric constant being dependent on atomic sizes or M–X distance (see eq. (7)). K is a quantity (see later) that is dependent on whether M is an atom of a metallic or of an insulating element (at NTP). The calculated value d_{XX} from eq. (6) may now be treated virtually as an '*ab initio*' quantity dependent only on 'portable'[15] core atomic size of M and X atoms (eq. (1)).

The best fits to plots (not shown) of d_{XX}(obs) vs d_{XX} (calcd) (κ = 1 in eq. (6)) in more than 160 gas-phase MX_2, MX_3 and MX_4 compounds give (R > 0.99) d_{XX} (obs) = 1.19d_{XX} (cal) – 15.8(9.2) for type I compounds and d_{XX} (obs) = 1.04d_{XX} (cal) – 6.7 for type II compounds. The improvement in the R factor of the fits as compared to that in Figure 1 attests to the goodness of the model (eq. (6)) especially considering that the gas-phase distances are obtained at various conditions of measurement, temperature and pressure and without a substantial theoretical basis for the 'core' atomic sizes. The finite intercepts of the best fits using eq. (6) highlights the uncertainty in the way κ of eq. (6) varies with atomic size.

Because of increase in polarizability with size, κ is expected to increase when κ is treated as an effective dielectric constant. We have varied κ as $\kappa = 1 + (Ld^{00}_{MX})^2$ such that the intercept of the best fit is zero. We find that L ~ 0.001 (for d^{00}_{MX} in pm) is empirically required for all compounds we thus write

$$d_{XX}\ (\text{calcd}) = 2\{1 + (0.001d^{00}_{MX})^2\}KCR_0^-(X)/(2 - 1.414t^{\pm}_{00}). \qquad (7)$$

The best fits to plots (see Figure 2) of d_{XX} (obs) vs d_{XX} (calcd) (using eq. (7)) gives

$$K\ (\text{type I})/K\ (\text{type (II)}) \approx 1.08. \qquad (8)$$

We have thus chosen K = 1 for type II compounds and K = 1.08 for type I compounds in eq. (7). The calculated values of d_{XX} is comparable to results from theoretical calculations[12] (standard deviation is 8 pm for type II and 13 pm for type I).

It is of fundamental interest to understand changes in K for type I (M = metal) and type II (M = insulator) compounds. The size $2CR_0^-(X)$ ($K = 1$ in eq. (2)) is close[9] to the negatively charged ionic radii of atoms in solids while the size $2 \times 1.08 \times CR_0^-(X)$ ($K = 1.08$ in eq. (2)) could be close to the so-called van der Waals' radii[11], r_{VDW}. For example, the ratio of the Bondi radii[11] of r_{VDW} for C, N, O, F to the corresponding values of $CR_0^-(X)$ is close to 1.09. The nearest-neighbour interatomic separation of Ne, Ar, Kr and Xe in their crystals[17] when given by $2 \times 1.08 \times CR_0^-(X)$ could require r_G values of 0.27, 0.51, 0.61 and 0.74 (a.u.), respectively, which is close to that expected (e.g., from the Zunger–Cohen valence s-electron radii[18] of 0.22, 0.46, 0.65 and 0.75 (a.u.)).

A point of importance[4] is the relative insensitivity of non-bonded $X- - -X$ distances to the deviation of bonded $M–X$ distances from the calculated value of d_{MX}^{n0} (using eq. (1)) is shown in Figure 3. The invariant 1,3-XX non-bonded distances may be regarded as struts and the variable 1,2-MX distances may be regarded as tensile elements for molecular tensegrity structures of gas-phase MX_n compounds. This is consistent with early seminal observations of Bartell[19], re-emphasized by Gillespie and coworkers[14,15]. The invariance of 1,3-non-bonded distances may be regarded as struts and the more variable 1,2-distances as tensile elements in molecular tensegrity structures of gas-phase MX_n compounds. Our methodology is applicable to terminal linkages in gas-phase dimers (such as those in M_2X_6 dimers, M = Al, Ga, X = halogen) or organic compounds but not to the bridged linkages (showing effects due to a transition to a condensed state). The main exceptions (not shown) are the linear compounds KrF_2 and XeF_2 and the axial non-bonded $F- - -F$ distances in T-shaped molecules, BrF_3 and ClF_3. The understanding of non-bonded $X- - -X$ distance using eq. (5) for these and other $n > 4$ MX_n compounds requires more elaboration.

In conclusion, we find that molecular tensegrity seems to be a powerful concept for molecular structure. Our methodology does not require prior knowledge of ionic character of $M–X$ bond, or the full weight of complex quantum chemical calculations given a core atomic size.

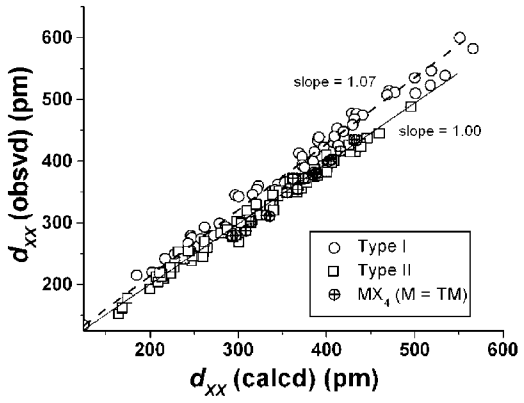

Figure 2. Plots of d_{XX} (obs) vs d_{XX} (calcd) using eqs (7) and (8) ($K = 1$ for type II compounds; for transition metal tetrahalides, we take $\kappa = 1$). The best fits ($R > 0.993$) give d_{XX} (obs) = $1.07d_{XX}$ (calcd) for type I compounds and d_{XX} (obs) = $0.99d_{XX}$ (calcd) for type II compounds

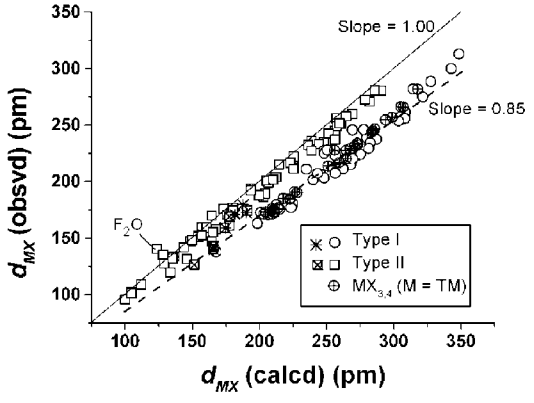

Figure 3. Plots of d_{MX} (obs) of gas-phase MX_n compounds ($n \geq 4$) (refs 12, 13) vs d_{MX}^{n0} (calculated) using eq. (1). Type I compounds indicated by a star are compounds such as AlH_2, SnH_4, PbH_4. Type II compounds with a cross are compounds which show $M–X$ double bond character such as SO_2, SO_3, BO_2.

1. Ganguly, P., Molecular geometry from molecular tensegrity: A case study of gas-phase $MX2$ compounds. *Curr. Sci.*, 2006, **90**, 1251–1253.
2. Fuller, R. B., *Synergetics, Explorations in the Geometry of Thinking*, Collier Macmillan, London, UK, 1975; Letter written by Buckminster Fuller to Robert Burhardt dating from February 2 to March 18, 1982 and found on the web site of the Buckminster Fuller Institute (www.bfi.org).
3. Ingber, D. E., Heidemann, S. R., Lamoureux, P. and Buxbaum, R. E., Opposing views on tensegrity as a structural framework for understanding cell mechanic. *J. Appl. Physiol.*, 2000, **89**, 1663–1678
4. Ganguly, P., Molecular geometry from molecular tensegrity: A case study of gas-phase MX_2 compounds. *Curr. Sci.*, 2006, **90**, 1251–1253; we repeat some of the eqns here for the sake of continuity.
5. Ganguly, P., Atom-bond transition: Transferability of atomic length scales. *J. Phys. Chem. A*, 2000, **104**, 8432–8444.
6. See, for example, Politzer, P. and Murray, J. S., The fundamental nature and role of the electrostatic potential in atoms and molecules. *Theoret. Chem. Acc.*, **2002**, 108, 134 and references therein.
7. Goldschmidt's tolerance factor in MBX_3 perovskites is given as $t = d_{MX}/\sqrt{2}d_{BX} \equiv d_{MX}/d_{XX}$; see Ganguly, P. and Shah, N., *Physica C*, 1993, **208**, 307 and references therein.
8. See Simon, A., Intermetallic compounds and the use of atomic radii in their description. *Angew. Chem.*, 1983, **95**, 94–113; *Int. Ed. Eng.*, 1983, **22**, 95–113.
9. Ganguly, P., Orbital radii and environment-independent transferable atomic length scales. *J. Am. Chem. Soc.*, 1995, **117**, 1776.
10. See Ganguly, P., Relation between interatomic distances in transition-metal elements, multiple bond distances and pseudopotential orbital radii. *J. Am. Chem. Soc.*, 1995, **117**, 2656. For n_v 'unsaturated' (we prefer the term 'extrabonding') valence electrons $F_S \approx [1 + (2/\pi)^2\{S(S+1)\}^{1/3}] \approx 1, 1.18, 1.26. 1.32, 1.38$ an 1.46 for $n_v = 0, 1, 2, 3, 4$ and 5, respectively.
11. See, for example, Bondi, A., van der Waals volumes and radii. *J. Phys. Chem.*, 1964, **68**, 441–451.
12. See Hargittai, M., Molecular structure of metal halides. *Chem. Rev.*, 2000, **100**, 2233–2301 and references therein for a comprehensive review.

13. Interatomic distances are obtained from *CRC Handbook of Chemistry and Physics* (ed. Weast, R. C.), CRC Press, Boca Raton, 1980, 61st edn, F-221.
14. Gillespie, R. J. and Robinson, E. A., Models of molecular geometry. *Chem. Soc. Rev.*, 2005, **34**, 396–407.
15. See Robinson, E. A. and Gillespie, R. J., Ligand close packing and the geometry of the fluorides of the nonmetals of periods 3, 4, and 5. *Inorg. Chem.*, 2003, **42**, 3865–3872.
16. Hoffmann, R., Qualitative thinking in the age of modern computational chemistry – or what Lionel Salem knows. *J. Mol. Struct. (Theochem.)*, 1998, **424**, 1.
17. See Wyckoff, R. W. G., *Crystal Structure*, Interscience Publishers, 1964, 2nd edn, vol. 1, Chapter II.
18. See Zunger, A., Systematization of the stable crystal structure of all AB-type binary comounds: A pseudopotential orbital-radii approach. *Phys. Rev. B*, 1980, **20**, 5839 and references therein.
19. See Bartell, L. S., A coordination chemist's entanglement with Gilespie's theories of molecular geometry. *Coord. Chem. Rev.*, 2000, **197**, 37.

ACKNOWLEDGEMENT. I thank the Council of Scientific and Industrial Research, New Delhi for an emeritus sustenance grant.

Received 19 May 2006; accepted 26 August 2006

Natural radioactivity of coal and its by-products in the Baoji coal-fired power plant, China

Xinwei Lu*, Xiaodan Jia and Fengling Wang

College of Tourism and Environment, Shaanxi Normal University, Xi'an 710062, P.R. China

Coal, bottom ash and fly ash from the Baoji coal-fired power plant, China were measured for ^{226}Ra, ^{232}Th and ^{40}K by a NaI(Tl) γ-ray spectrometer. The results show that fly ash or bottom ash contain three to six times more natural radionuclides than feed coal. The results are compared with the available data from other countries. Radium equivalent activity and external index are calculated for by-products to assess the radiation hazards arising due to the use of these ash samples in the construction of dwellings. Some fly-ash samples have radium equivalent activities and external hazard index values more than 370 Bq kg^{-1} and unity respectively. The absorbed dose rate at 1 m above the ash pond was (155 nGy h^{-1}) higher than the global average value of 55 nGy h^{-1} and the Chinese average value of 81.5 nGy h^{-1}. The corresponding annual external effective dose is estimated to be 0.191 mSv y^{-1}, which is less than that (0.46 mSv y^{-1}) in areas of natural background radiation.

Keywords: Bottom ash, coal, fly ash, natural radioactivity, γ-spectrometry.

THERE has been an increasing demand for electricity generation throughout the world with the ever-increasing growth in human civilization. With the increasing demand for electricity, coal plays an important role in electric power generation worldwide. China depends largely on coal reserves for energy needs, which contribute more than 70% of the total power generated at present in China[1]. Coal, burned as fuel material in power plants, produces energy and a large amount of solid waste. The solid waste resulting from coal combustion are mainly fly ash and bottom ash. Bottom ash is the coarse-grained material that is collected at the bottom of the boiler and fly ash is entrained in the gas stream and carried up the stack following combustion. Depending on the emission control system of the stack, most of the fly ash is recovered by collection devices and any leftover is released into the atmosphere and deposited on the soil around the coal-fired power plant. The ashes tend to be enriched in inorganic elements (metals and radionuclides).

Since the ashes produced may be either disposed-off or utilized further in other applications such as the building materials industry, it is important to study in detail, the radiological characteristics of the various fractions. Furthermore, detailed knowledge of the radiological characteristics allows better determination of the radiation exposure, both occupational and of the public, due to the produced ashes. Eisenbud and Petro[2] first pointed out that radiation dose from the use of fossil fuel for power generation could be a significant addition to the natural radiation dose. The natural radioactivity of coal and by-products from coal-fired power plant has been noticed in many countries. There are many studies on measurement of concentration of radionuclides in coal and ash or on the estimation of radioactive influence of coal-fired power plant to the ambient environment[3–17], but data for Baoji coal-fired power plant are lacking.

Baoji is the second largest city in the Shaanxi Province in central China. It is located at the western end of the central Shaanxi basin about 150 km west from the provincial capital, Xi'an city. Baoji is surrounded by mountains and plateau in the north, west and south. Only the east is open toward the lower reach of the Weihe River, a major branch of the Yellow River in Shaanxi Province. The Weihe River runs through the city from west to east. Baoji coal-fired power plant with a 60 m stack, situated at the western extremity of the city, has been in operation since 1960s. The power plant with 1.5×10^6 kWh annual production capacity consumes low-quality bituminous coal reserves from Tongchuan of Shaanxi and Huating of Gansu, and produces approximately 4500 tonnes (t) of fly and bottom ash per day from more than 14,000 t of coal. The ash content in the bituminous coal reserve used at the Baoji power plant is in range 12.12–38.82%. There are two big ash ponds (about 1000 m length, 500 m width and 25 m depth) for deposited ash from ash-water. The ash from this power plant is mainly used in producing cement and other building materials or aggregate in stabilizing roadways.

*For correspondence. (e-mail: luxinwei@snnu.edu.cn)